

Flow Physics of a Porous Cylinder

Prabin Paudel¹ and Chandan Bose²

¹Department of Mechanical and Aerospace Engineering, Pulchowk Campus, Institute of Engineering,
Tribhuvan University

²Assistant Professor, Aerospace Engineering, College of Engineering and Physical Sciences, The
University of Birmingham

September 18, 2024

Synopsis

This study investigates the flow physics and wake dynamics around porous and solid circular cylindrical blockages using 2D numerical simulations at Reynolds numbers 50 and 100. Permeability, which determines the ease with which fluid traverses a porous medium, is a fundamental parameter for understanding and predicting flow behaviour around these blockages. The project aims to compare the flow through a porous blockage with flow past a solid blockage at Darcy numbers ranging from 10^{-9} to 0.1, with a detailed focus at a Darcy number of $1/500$. The goal is to understand flow patterns, force coefficients, and wake dynamics for both types of blockages. The study reveals that at Reynolds number 50, both blockages exhibit steady flow, with porous blockages having a slightly larger re-circulation region. At Reynolds number 100, the flow becomes unsteady, with porous blockages demonstrating greater stability but higher drag coefficients compared to solid blockages. These findings enhance the understanding of flow behaviour around porous structures, which is vital for applications in filtration, aerodynamics, and environmental engineering.

1 Introduction

Porous blockage refers to a condition in fluid dynamics where a flow passes through an obstacle or a medium that contains numerous small openings or pores. Unlike solid blockages, which completely obstruct fluid flow, porous blockages allow a portion of the fluid to pass through while the rest flows around the obstacle. Studies focusing on flow around bluff bodies are of interest due to their academic value and the engineering importance related to structural design and flow-induced vibrations. Research on flow around cylinders mainly centers on square and circular shapes. In the case of steady flow over a circular cylinder, the flow features and characteristics are determined by the Reynolds number. Available literature offers both experimental and numerical data on parameters like separation angles, velocity distribution, wake lengths, pressure coefficients and drag

coefficients [1, 2].

Permeability of a medium, which dictates how easily fluid can pass through it, is a critical parameter in understanding and predicting the flow behaviour around such blockages. Porous blockages are encountered in various natural and industrial contexts. In nature, examples include vegetation in a river, coral reefs in ocean currents, and the porous exoskeletons of certain marine animals. In engineering, porous materials are used in filters, heat exchangers, and as structural components in aerodynamic applications. The study of flow around a dandelion seed revealed a ring of detached recirculating fluid, which is key to understanding pappus-mediated flight [3]. Direct numerical simulation on a 2D grid has previously been used to study viscous flow across a thick permeable circular disk between the ranges of the Reynolds number (Re) of 10 to 130 and the Darcy number (Da) of 10^{-9} to 1. Three different regimes, effectively impervious, transition and highly permeable regimes depending on Darcy number, have been observed and characterized [4].

This study aims to investigate the constant flow through and past a solid cylinder and a porous circular cylinder. We conduct detailed examinations of how flow patterns, specifically the wake structure, change with Reynolds and Darcy numbers. This work is somewhat comparable to earlier studies conducted by Bhattacharyya et al. [5] and Noymer et al. [6], which examined steady flow through a porous circular cylinder across a broad range of Reynolds and Darcy numbers. The flow field behind a porous blockage is normally studied using a numerical model based on the Darcy-Brinkman equations [7] and Darcy-Brinkman-Forchheimer equations [8]. In this study, we will be using the former.

2 Governing Equations and Models

2.1 Problem definition

This study investigates the flow physics and wake dynamics of a porous circular cylindrical blockage compared to a solid cylindrical blockage at Reynolds numbers of 50 and 100 at various Darcy numbers using 2D numerical simulations. This study aims to compare the study of flow past and through a porous blockage with solid blockage at Darcy number ($1/D$) in the range of 10^{-9} to 0.1 while the detailed study is done at Darcy number of $1/500$. The study details variations in flow pattern and force coefficient experienced by porous and solid blockage under different Reynolds numbers and Darcy numbers.

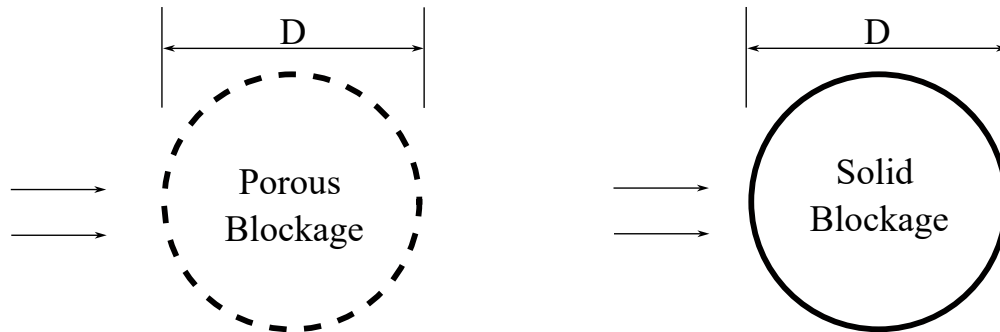


Figure 1: Schematic diagram of Porous and Solid circular cylindrical blockage

2.2 Governing equations

let us consider a cylindrical porous blockage with diameter D , isotropic porosity ϵ permeability k in a fluid flow with velocity U , density ρ , ν as kinematic viscosity and p is the pressure. The non-dimensional continuity equation,

$$\nabla \cdot \mathbf{u} = 0 \quad (1)$$

is solved in the entire fluid domain. While the non-dimensional Navier-Stokes equation for incompressible fluid flow,

$$(\mathbf{u} \cdot \nabla) \mathbf{u} = -\nabla p + \frac{1}{Re} \nabla^2 \mathbf{u}, \quad (2)$$

is solved in the flow domain, the Darcy-Forchheimer equation,

$$\frac{1}{\epsilon^2} (\mathbf{u} \cdot \nabla) \mathbf{u} = -\nabla p + \frac{1}{\epsilon Re} \nabla^2 \mathbf{u} - \frac{1}{Da Re} \mathbf{u} \quad (3)$$

is solved in the porous region where,

$$Re = \frac{U \rho D}{\mu} \quad (4)$$

,

$$Da = \frac{k}{D^2} \quad (5)$$

are Reynolds's number and Darcy's number, respectively.

2.3 Geometry and Mesh

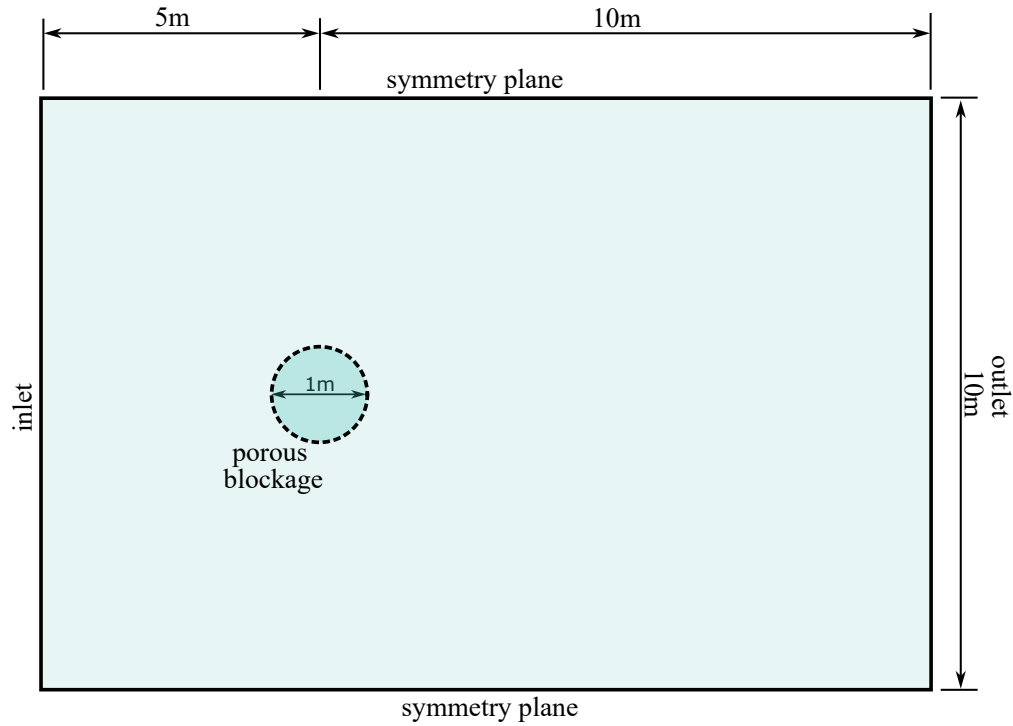


Figure 2: Computational domain for porous case

The computational domain used for the study is a simple rectangular domain with cylindrical porous blockage and a solid cylinder for porous and solid cases respectively. blockMesh utility in the OpenFOAM framework is used to construct this computational domain. The cylindrical blockage has a diameter of $D = 1m$. The computational domain is $15D$ in streamwise direction and $10D$ in normal direction as shown in figure 2 with the origin lying at the centre of the cylindrical blockage. The computational domain for the solid case is similar in dimensions with solid blockage in place of porous blockage.

A grid convergence test is done to finalize the grid size for both porous as well as solid cases, which is detailed in section 3.1.1. The final converged mesh for porous and solid cases is shown in figure 3 and 4, respectively.

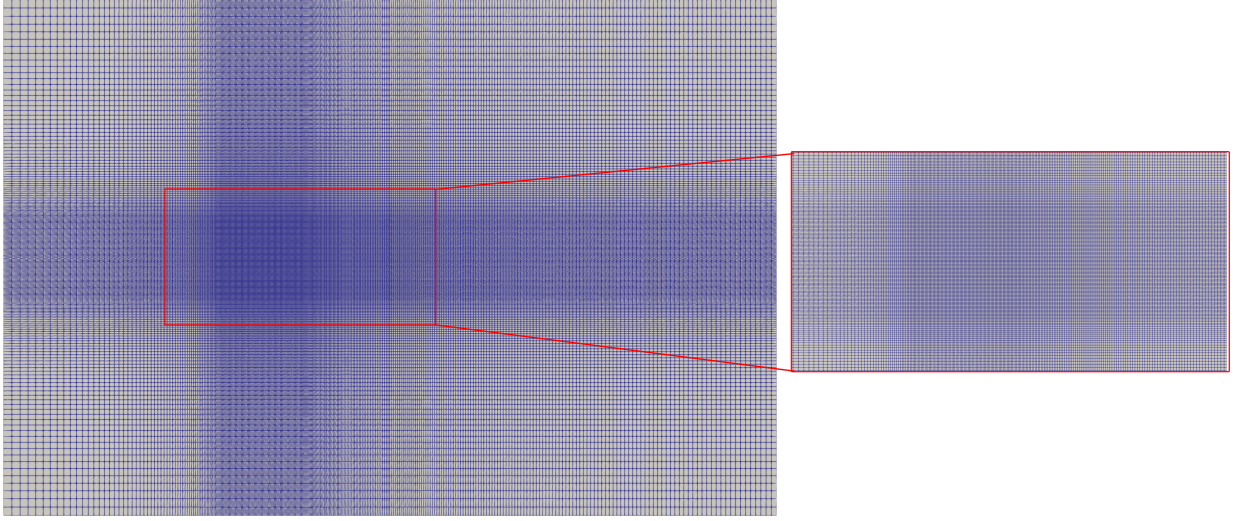


Figure 3: Computational mesh for porous blockage case

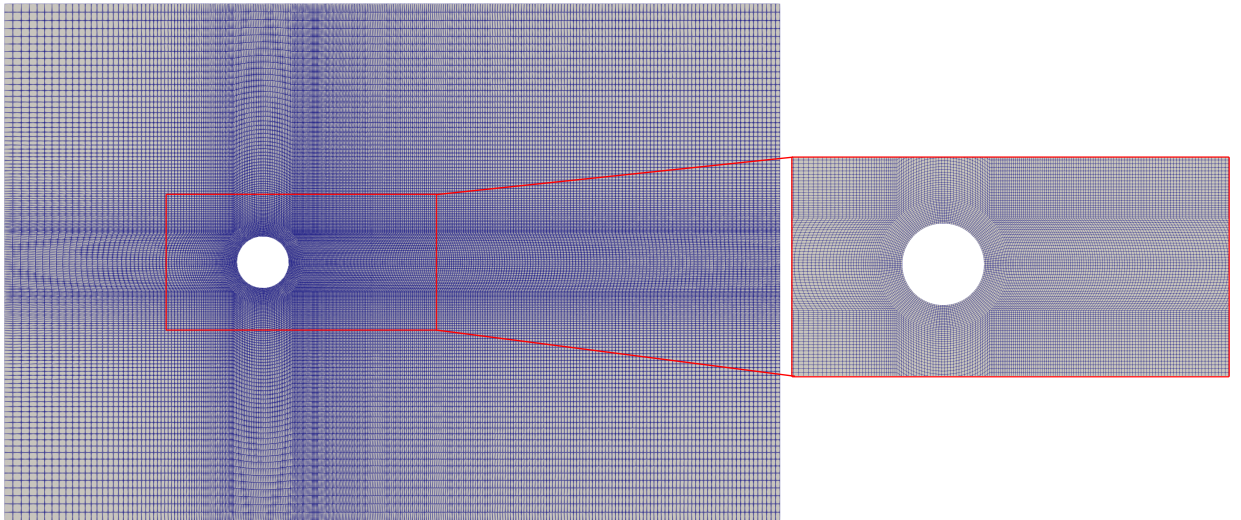


Figure 4: Computational mesh for solid blockage case

2.4 Initial and Boundary Condition

2.4.1 Fluid Properties

This case study is done for two Reynolds numbers of 50 and 100, and the initial flow conditions are set accordingly. Inlet velocity is defined as 0.25m/s and 0.5m/s for Reynolds's numbers 50 and 100, respectively. Other relevant flow properties are tabulated below.

Table 1: Initial Flow Conditions

Flow variables	Value
ρ	1 kg/m^3
ν	$5e-3\text{ m}^2/\text{s}$

2.4.2 Boundary Conditions

The boundary conditions used for both the cases of porous and solid blockage are as tabulated below.

Table 2: Boundary Conditions for Porous Blockage

Domain	Pressure	Velocity
inlet	zeroGradient	fixedValue
outlet	fixedValue	pressureInletOut- letVelocity

Table 3: Boundary Conditions for Solid Blockage

Domain	Pressure	Velocity
inlet	zeroGradient	fixedValue
cylinder	zeroGradient	noSlip
outlet	fixedValue	pressureInletOut- letVelocity

2.5 Solver Selection

PisoFoam solver is chosen for the numerical analysis on the grounds that the flow is incompressible, laminar, and transitory in nature. pisoFoam is a builtin pressure based solver in OpenFOAM for laminar incompressible transient flow problems using PISO algorithm.

2.6 Discretization Schemes

The discretization schemes used in the laminar viscous simulation are as tabulated in table 4.

Table 4: Discretization Schemes for Viscous Simulations

Parameters	Discretization Scheme	Order of accuracy
Time Derivative	Euler	First order
Gradient	Gauss Linear	Second order
Divergence	div(phi,U): Gauss LUST grad(U)	Second Order
	Viscous stress tensor: Gauss linear	Second Order
Laplacian	Gauss Linear uncorrected	Second Order
Interpolation	linear	First Order

2.7 Solution Method and Control

The pressure field is solved using the Geometric-Algebraic MultiGrid (GAMG) solver with a tolerance of $1e-08$ and a relative tolerance of 0.0001 , using Gauss-Seidel smoothing. For the final pressure solution, the relative tolerance is set to zero for higher accuracy. Velocity (U) is solved with the ‘smoothSolver’ using Gauss-Seidel smoothing, an absolute tolerance of $1e-08$, and zero relative tolerance. The PISO algorithm is configured with two corrector steps, no non-orthogonal correctors, and references the first cell with a pressure value of zero for stability. This setup ensures efficient and accurate solution convergence for pressure and turbulence in transient simulations.

3 Results and Discussions

3.1 Convergence Tests

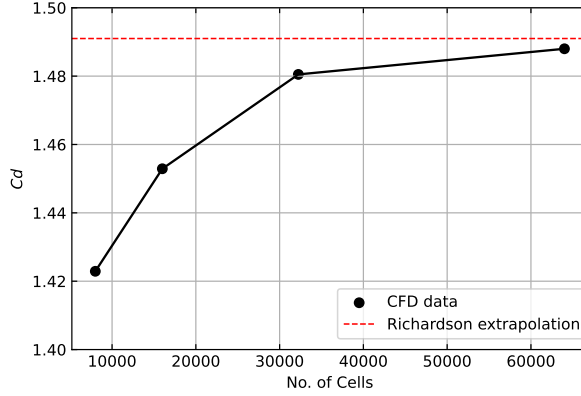
Grid size convergence test was done for both computational grids of porous and solid blockage. Test was done for Reynolds no of 100 so that the converged grid still maintains targeted y^+ values for Reynolds number 50 as well. Also the Darcy number of $1/500$ is used for the grid convergence study.

3.1.1 Grid Size Convergence Test

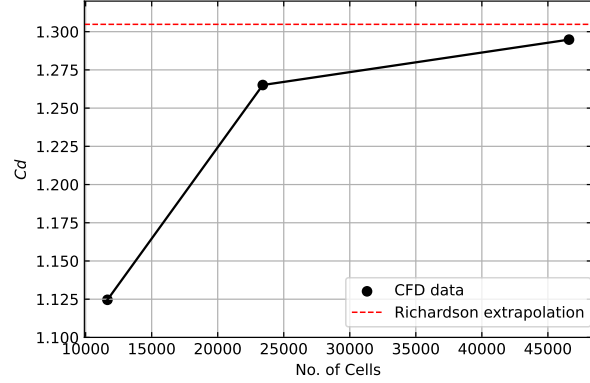
Grid convergence test was done with three different sets of mesh differing by a factor of 2. The drag coefficient (C_d) value, before the onset of unsteadiness, was selected as the convergence parameter for both cases. Then Richardson extrapolation method was employed to determine the converged value of the drag coefficient (C_d) as both Δx and Δy approach zero using the reference provided in [9]. The drag coefficient’s converged value, or C_d , is shown in the table below.

Table 5: Converged value of C_d

Re	Porous blockage	Solid Blockage
100	1.4910	1.3048



(a)



(b)

Figure 5: Grid Convergence study for (a) porous and (b) solid blockage computational meshes

Table 6: Grid Convergence Study for Porous Blockage

Grid	Number of cells	Drag Coefficient(C_D)	Percentage error
—	8000	1.4229	4.567%
Coarse	16000	1.4529	2.555%
Medium	32234	1.4805	0.704%
Fine	64000	1.4880	0.201%

Table 7: Grid Convergence Study for Solid Blockage

Grid	Number of cells	Drag Coefficient(C_D)	Percentage error
Coarse	11650	1.1246	13.81%
Medium	23412	1.2651	3.043%
Fine	46600	1.2948	0.766%

Calculations were made using a factor of safety of 1.25 to determine the grid convergence index (GCI). Convergence criteria were set $G.C.I < 0.1$. For porous blockage cases, With medium to fine transition having $G.C.I = 0.0025$, and medium mesh having an error of 0.704%, medium mesh with 32234 cell numbers was considered converged. For solid blockage cases, with medium to fine transition having $G.C.I = 0.0393$, and fine mesh having an error of 0.766%, fine mesh with 46600

Table 8: Grid Convergence Index

Grid-transition	G.C.I(Porous case)	G.C.I (Solid case)
Coarse-Medium	0.0025	0.0097
Medium-Fine	0.0088	0.0393

cells was considered converged. However, for the porous case to keep the mesh parameters like Δx and Δy similar to the solid blockage case, the computation was carried out in fine mesh. Parameters of converged mesh are tabulated in table 9, figure 3 and figure 4 illustrate converged mesh.

Table 9: Parameters of Converged Mesh

Number of cells	min $\Delta x(m)$	min $\Delta y(m)$
46600(solid)	0.020	0.022
64000(porous)	0.020	0.020

3.2 Results

3.2.1 Reynolds number = 50

In this section, we will be comparing the wake behind porous blockage with Darcy number ($D = 1/500$) and solid blockage at Reynolds number of 50. In figure 6, velocity contour and the streamlines behind the porous blockage is shown, comparing it to the velocity contour and streamlines around the solid blockage in figure 7, the flow features are very similar in nature in both the cases. The flow is separated, and a re-circulation region is formed, but it is steady in nature in both cases. The re-circulation region is slightly bigger in the porous case with a reattachment length of 2.79 m compared to 2.65m in solid blockage.

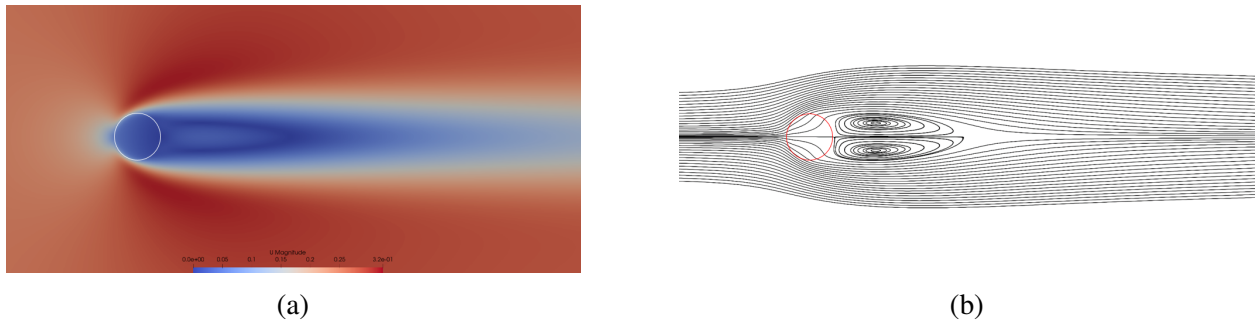


Figure 6: Flow field around porous blockage at $Re = 50$ (a) velocity contour of the flow field (b) streamlines on the flowfield where red/white circles represent the position of the porous blockage

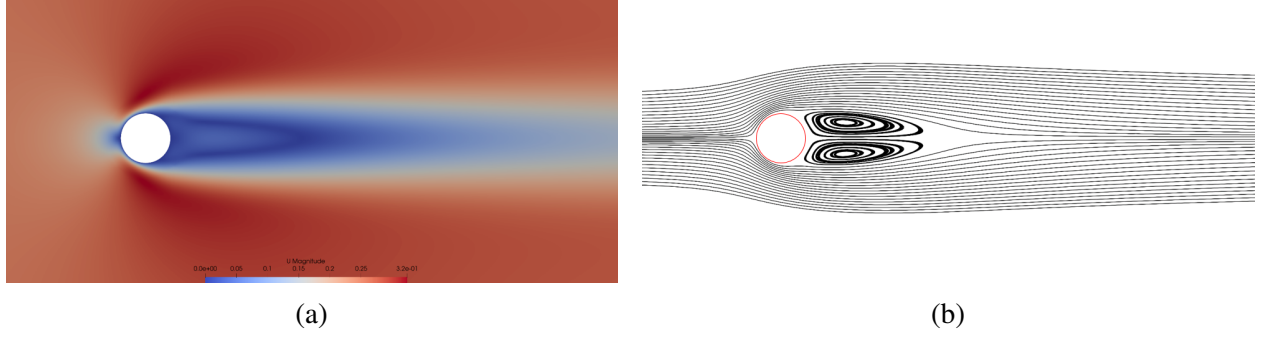


Figure 7: Flow field around solid blockage at $Re = 50$ (a) velocity contour of the flow field (b) streamlines on the flowfield where red/white circles represent the position of the porous blockage

Steady nature of the flow is more evident in figure 8 and 9 as the drag coefficient (C_d) attains constant value and as the lift coefficient (C_l) remains 0 in both the cases. The drag coefficient for porous blockage is 1.695 which is slightly greater than for solid blockage, 1.643.

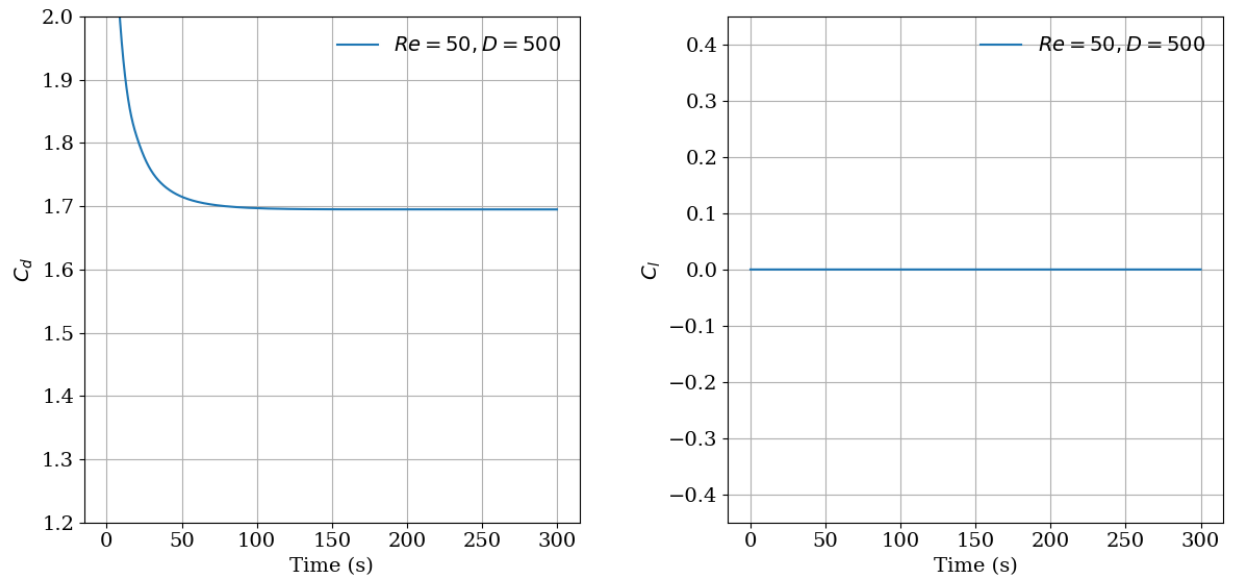
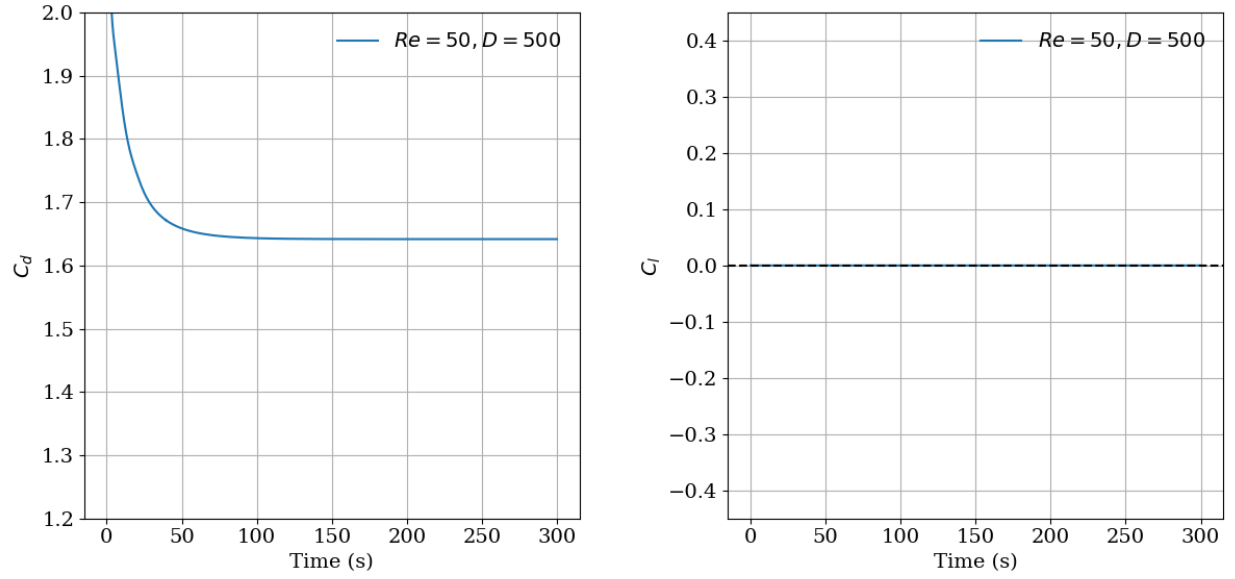
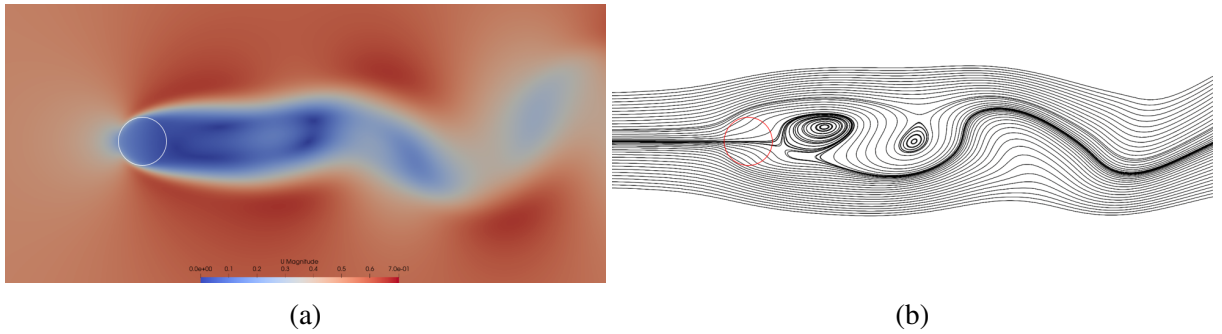


Figure 8: C_d and C_l evolution over time for porous blockage

Figure 9: C_d and C_l evolution over time for solid blockage

3.2.2 Reynolds number = 100

In this section, we will be comparing the wake behind porous blockage with Darcy number ($D = 1/500$) and solid blockage at Reynolds number of 100. The wake behind both solid and porous blockage is, however, unsteady in this case, as evident in velocity contour and streamlines behind the porous blockage in figure 10 and 11.

Figure 10: Flow field behind around blockage at $Re = 100$ (a) velocity contour of the flow field (b) streamlines on the flowfield, where red/white circles represent the position of the porous blockage

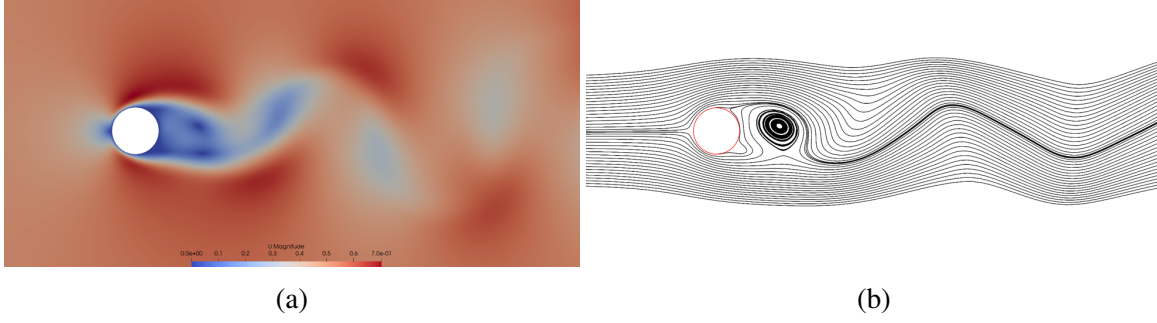


Figure 11: Flow field around solid blockage at $Re = 100$ (a) velocity contour of the flow field (b) streamlines on the flowfield

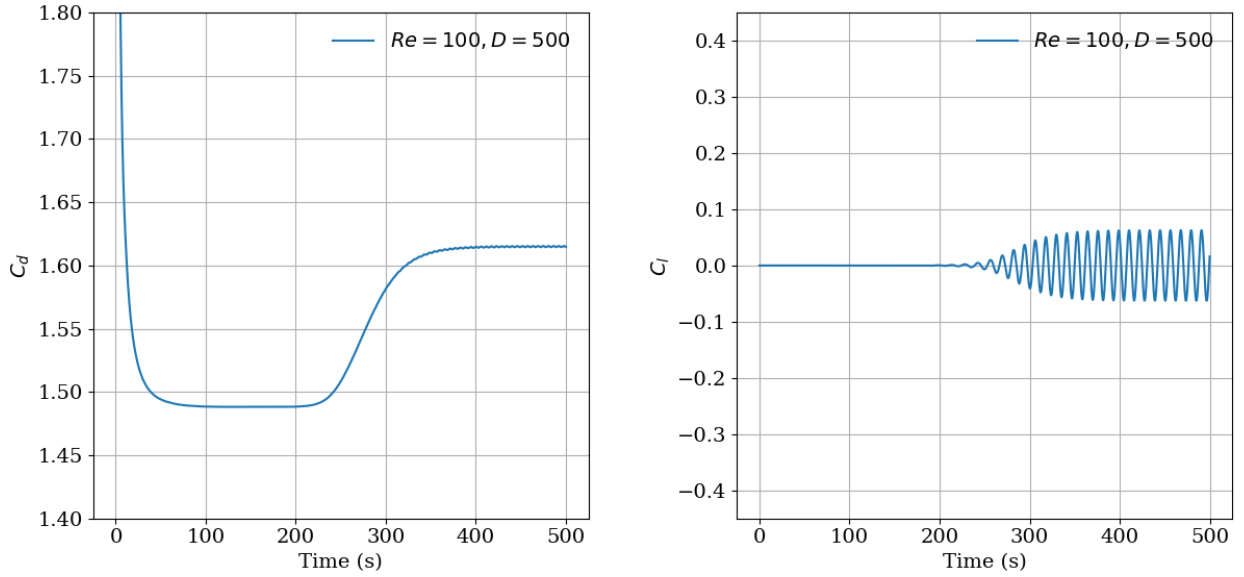
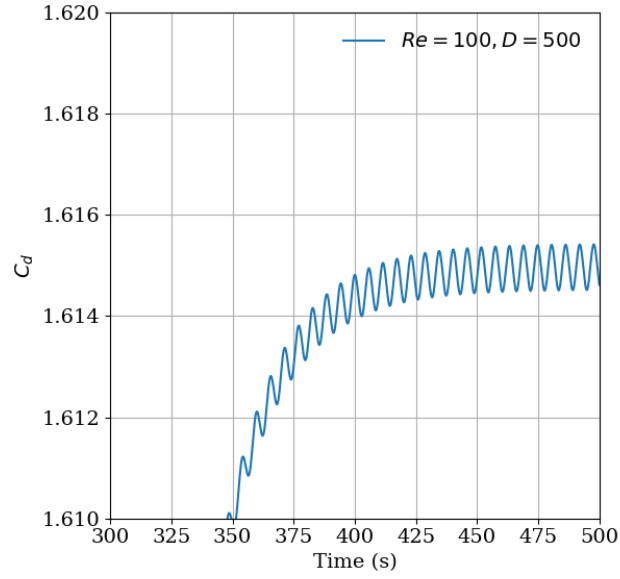
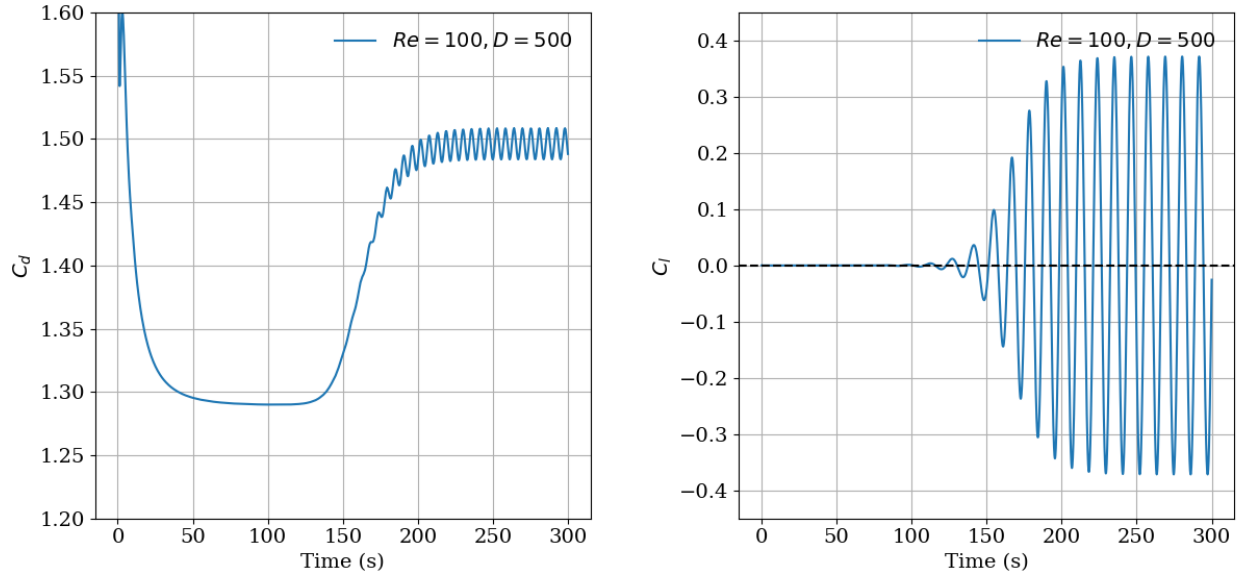


Figure 12: C_D and C_l evolution over time for porous blockage

The unsteady nature of the wake can be studied more with C_d plot evolution. As shown in figure 12 and 13, unsteadiness in the wake starts only after a certain time, and the onset is quicker on the solid blockage. Unsteadiness in the wake can be observed earlier in C_l plot i.e. in the force coefficient taken in the direction normal to the flow. C_d is higher in porous blockage both before and after the onset of unsteadiness in the wake. However the C_l and C_d values oscillate with higher amplitude in solid blockage in comparison to porous blockage. The values of C_l and C_d before and after unsteadiness for both porous and solid blockage are tabulated below:

Table 10: Force coefficient values for $Re = 100$

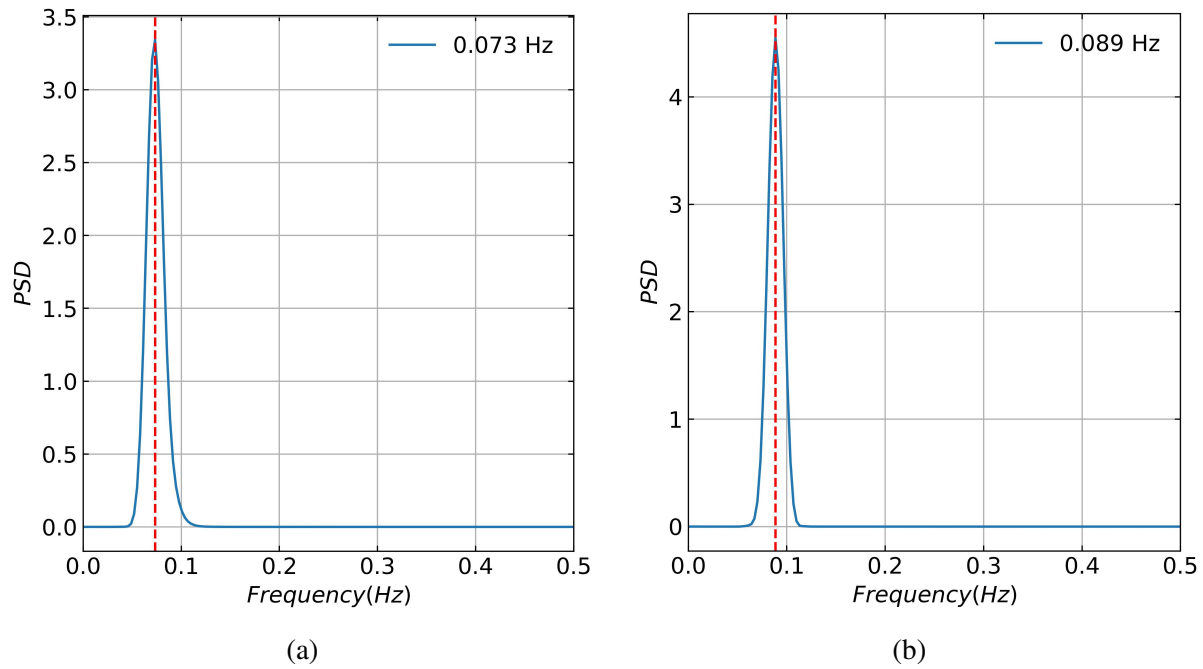
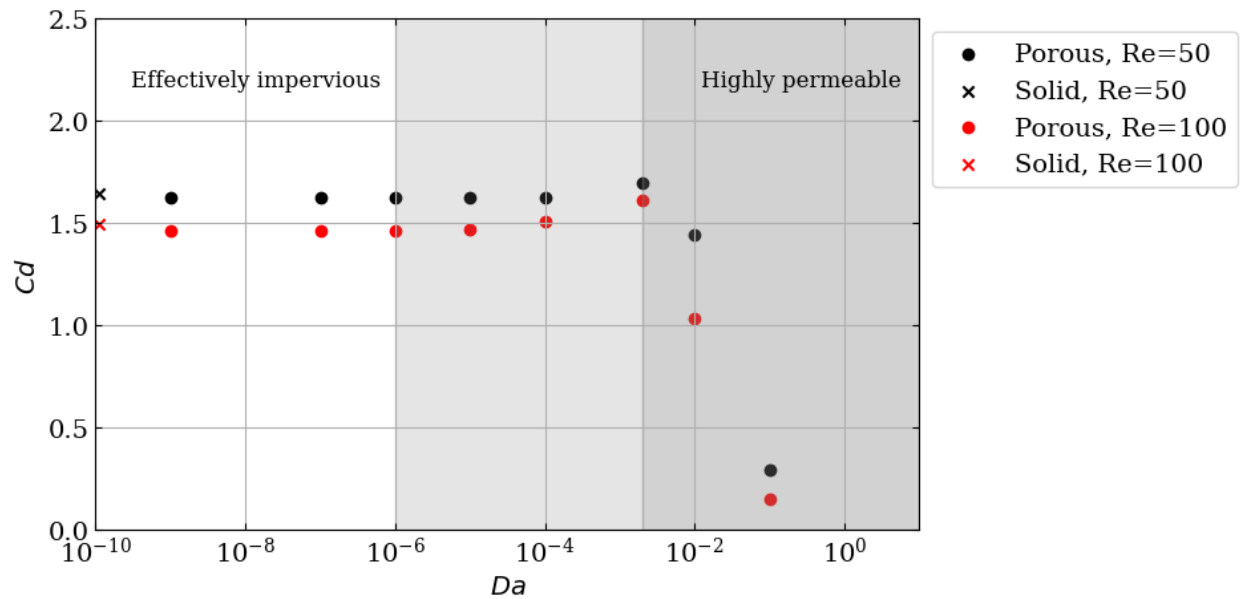
Force coefficients	Porous Blockage	Solid Blockage
C_d (before unsteadiness)	1.488	1.295
C_d (after unsteadiness)	1.614	1.495

Figure 13: C_D and C_l evolution over time for porous blockageFigure 14: C_D and C_l evolution over time for solid blockage

The nature of oscillation can be more studied with the Power Spectral Density (PSD) plot as shown in figure 15. The amplitude of oscillation is slightly greater in solid blockage, as evident in the PSD plot as well, and the same goes for the frequency of oscillation, which is slightly larger for solid blockage (0.089 Hz) compared to 0.073 Hz as for porous blockage.

Table 11: Force coefficient oscillation amplitude for porous and solid blockage

Force coefficients	Porous Blockage	Solid Blockage
C_d	4.5e-5	0.012
C_l	0.063	0.381

Figure 15: Power spectral density plot of C_l for (a) porous blockage and (b) solid blockageFigure 16: C_d vs Da for porous and solid blockage

In both cases of Reynolds numbers 50 and 100, C_d is greater for porous blockage than for solid blockage. This is a particular case of permeability as the Darcy number ($1/D$) of $1/500$ lies in the transition region of permeability as the blockage transitions from effectively impervious to highly permeable case. Figure 16 presents the results of an examination of the viscous flow over a porous circular disk in the Reynolds number (Re) range of 50, 100 and in the Darcy number (Da) range of 10^{-9} to 0.1. For majority of Darcy number C_d is smaller for porous blockage than solid blockage however as permeability transitions to highly permeable there is slight rise in the value of C_d before it dips to lower values. This is consistent with results obtained by Cummins et al. [4] on permeable disks and Yu et al. [8] on similar cylindrical blockage as in this study.

4 Conclusions

The results of this study reveal distinct differences in wake dynamics and force coefficients between porous and solid cylindrical blockages. At Reynolds number 50, both blockages exhibit steady flow with a larger re-circulation region (by 5.283%) and larger drag coefficient C_d (by 3.1.65%) for the porous blockage. At Reynolds number 100, the flow becomes unsteady, with larger C_d (by 7.96%) after the onset of unsteadiness for porous blockage. However, higher oscillation amplitudes were observed in solid blockages for both C_l and C_d . The drag coefficient (C_d) is generally higher for porous blockages across both Reynolds numbers, with the porous blockage showing greater stability in wake oscillations. In the Darcy number range of 10^{-9} to 0.1, C_D is greater for solid blockage for the majority of the number. The transition from effectively impervious to highly permeable states demonstrates a notable increase in C_d for porous blockage in comparison to solid blockage before dipping to lower values. These findings underscore the impact of permeability on flow behaviour, highlighting the nuanced differences in fluid dynamics between porous and solid structures.

5 Acknowledgements

I would like to express my profound gratitude to Prof. Chandan Bose at the University of Birmingham, whose unwavering support and guidance have been the cornerstone of my internship journey. A special thanks to Mr. Sanjay Ramachandran, whose assistance in navigating challenges and answering my queries has been invaluable. Lastly, I am deeply appreciative of Ms. Payel Mukherjee and the dedicated FOSSEE team at IIT Bombay for their support and for granting me this incredible internship opportunity.

References

- [1] B. Fornberg, “A numerical study of steady viscous flow past a circular cylinder,” *Journal of Fluid Mechanics*, vol. 98, no. 4, pp. 819–855, 1980.
- [2] A. Sohankar, C. Norberg, and L. Davidson, “Low-reynolds-number flow around a square cylinder at incidence: study of blockage, onset of vortex shedding and outlet boundary condition,” *International journal for numerical methods in fluids*, vol. 26, no. 1, pp. 39–56, 1998.
- [3] C. Cummins, M. Seale, A. Macente, D. Certini, E. Mastropaolo, I. M. Viola, and N. Nakayama, “A separated vortex ring underlies the flight of the dandelion,” *Nature*, vol. 562, no. 7727, pp. 414–418, 2018.
- [4] C. Cummins, I. M. Viola, E. Mastropaolo, and N. Nakayama, “The effect of permeability on the flow past permeable disks at low reynolds numbers,” *Physics of Fluids*, vol. 29, no. 9, 2017.
- [5] S. Bhattacharyya, S. Dhinakaran, and A. Khalili, “Fluid motion around and through a porous cylinder,” *Chemical Engineering Science*, vol. 61, no. 13, pp. 4451–4461, 2006.
- [6] P. D. Noymer, L. R. Glicksman, and A. Devendran, “Drag on a permeable cylinder in steady flow at moderate reynolds numbers,” *Chemical engineering science*, vol. 53, no. 16, pp. 2859–2869, 1998.
- [7] T.-C. Jue, “Numerical analysis of vortex shedding behind a porous square cylinder,” *International Journal of Numerical Methods for Heat & Fluid Flow*, vol. 14, no. 5, pp. 649–663, 2004.
- [8] P. Yu, Y. Zeng, T. S. Lee, X. B. Chen, and H. T. Low, “Steady flow around and through a permeable circular cylinder,” *Computers & Fluids*, vol. 42, no. 1, pp. 1–12, 2011.
- [9] A. S. of Mechanical Engineers. Fluids Engineering Division, *Quantification of Uncertainty in Computational Fluid Dynamics*. American Society of Mechanical Engineers, 1993.